

Registering High Resolution Microscopic Images with Different Histochemical Stainings - A Tool for Mapping Gene Expression with Cellular Structures

Lee Cooper¹, Shan Naidu², Gustavo Leone², Joel Saltz¹, Kun Huang¹

¹Department of Biomedical Informatics, Ohio State University, Columbus, USA

²The Comprehensive Cancer Center, Ohio State University, Columbus, USA

Abstract— One of the key problems in system biology is to develop realistic models for interaction between different types of cells with high resolution spatial information. Large scale microscopic imaging is an essential tool for this purpose since it can capture both cellular distribution as well as gene expression information. However, a difficult issue is how to integrate the information for cellular and molecular distributions which are usually obtained using different types of staining techniques on different histological sections. This problem is particularly challenging due to the large size of the microscopic images (usually in the size of several gigabytes per image). In order to solve this problem, we present an image registration workflow aligning microscopic images with different types of staining. This workflow contains three stages: rigid registration, nonrigid registration, and multiresolution refinement. The focus of this paper is to develop an efficient and scalable algorithm to obtain precise nonrigid registration results. We first established that the sharpness of the normalized cross-correlation function can be used as a similarity measure for matching corresponding points between two images. This helps us avoid the high computational cost in computing other measures such as mutual information, which is critical for processing images this large. The matched points are used as control points to compute nonrigid transformation between the two images. In order to improve the matching accuracy, we adopt a multiple resolution approach for accurately matching key regions of interests. We tested this algorithm using real histological images of mouse mammary gland samples by focusing the mammary gland duct which is the potential site for breast tumor initiation. The results show that our algorithm is highly accurate and will be applicable to a large scale gene expression mapping studies on breast tumor microenvironment.

I. INTRODUCTION

One of the key problems in the post genomic era is to understand the regulation of gene expressions in organisms. Proteomics techniques such as genechips

(microarray) and mass spectroscopy have provided a tremendous amount of information on gene expression patterns, however in most experiments these techniques are applied to biological samples that contain a diverse population of cells and therefore reflect “averaged” expression profiles. In contrast gene expression profiles in different types of cells can be drastically different and studies show that even the same type of cell in the same tissue microenvironment can exhibit heterogeneity in the expression levels of key proteins [15]. Therefore, the capability to map gene expression to individual cells is essential to explore gene regulation within tissue environments at the cellular level.

In this paper we present a method for mapping gene expression based on registration of high-resolution microscopic images with distinct staining types. For instance, given two serial sections from a mouse mammary gland one section is stained to identify cellular structure using specific immunohistochemical staining and the other section is stained for an important tumor suppressor gene *PTEN*. By registering these two section images we obtain the mapping of expression of *PTEN* in features of interest such as fibroblasts and epithelial cells.

To accomplish registration at the precision necessary for expression mapping three challenges need to be addressed: comparison across multiple modalities, nonrigid deformation and change in morphology between the two images, and the large size of histological images obtained at high magnification. In this paper we address these challenges with the following approaches:

- 1) Design a new similarity measure for matching feature points between two images with different staining. The goal of image registration is to determine a transformation that maximizes the similarity between two images. Mutual information (MI) and normalized cross correlation (NCC) are commonly used as similarity measures in registration. However, we found that for matching image

patches hard thresholds for the peak value of these similarity measures are not adequate to discriminate good matches in this scenario. Therefore we propose a new similarity measure based on the "sharpness" of the cross-correlation function.

- 2) Adopt a multiple resolution approach for nonrigid transformation. In order to register the images as precisely as possible a large amount of matched control points are required to compute an accurate mapping between them. Due to the elasticity and heterogeneity of the tissues in the biological sample the local transformation cannot be extrapolated globally. Therefore for the regions of interest, we implement a local multiple resolution matching approach to align these regions in a piecewise linear manner.
- 3) Develop a scalable image registration framework. Microscopic images can be very large. Using an Aperio slide scanner to scan a $1.5\text{cm} \times 3\text{cm}$ section at 20X objective length generates an image at the resolution $0.5\mu\text{m}/\text{pixel}$ that is $30,000 \times 60,000$ pixels and 6.5 GB in uncompressed form. These large sizes require algorithms that are scalable and parallelizable. Currently studies on parallel image registration algorithms are still rare [13]. Our algorithm uses scalable operations and has a highly parallelizable workflow.

Biological applications: In this paper our application focuses on a transgenic mouse model the *PTEN* gene knocked out in mammary gland fibroblast cells.¹ *PTEN*, also known as phosphatase and tensin homolog, is a well known tumor suppressor gene. Inactivation of *PTEN* is associated with several diseases including cancer [6]. It has been observed that this strain of mice inevitably develop epithelial breast tumor after the knockout. Therefore the critical question is to how the inactivation of the tumor suppressor gene *PTEN* in fibroblasts leads to tumor development in epithelial cells. Answering this question will provide critical insight on cell interaction and tumorigenesis in the tumor microenvironment. To answer these questions it is critical to obtain a series of spatial maps of expression levels of key genes in different types of cells.

The *PTEN* mapping is demonstrated using serial mammary tissue sections obtained from the transgenic mice with hematoxylin and eosin staining (H+E) and *PTEN* staining applied alternately to produce a sequence of sections with interleaved stain types. Section V contains the results of our registration algorithm applied to compute

the mapping for one such pair of sections.

Related work: There are many works on observing the expression map of a specific gene in cells. The most direct approach is to use confocal microscopic imaging to visualize the co-expression of the gene product and the cell specific markers, however this approach requires extensive molecular and genetic manipulation on the model animal system. In [12], a tissue microarray (TMA) approach was developed where small samples of retina ($0.5\text{mm} \times 0.5\text{mm}$) were fixed in plastic and sectioned at 250nm interval. Each section was stained for a special molecule of interest using immunochemical staining. Therefore for a section of sample of $5\mu\text{m}$ thick, the products of twenty different genes can be determined. A limit of this approach is that it is difficult to extend this technique to larger samples in the multiple-millimeter scale. Another approach to obtain gene expression profile at high spatial resolution is to use laser capture microdissection (LCM) to carve out small piece of tissue in each section and conduct microarray analysis on the carved samples. This way the entire profile of gene expression can be mapped to a spatial resolution of tens of microns. Other approaches to obtain the gene expression information for multiple genes include multiple spectral imaging [2], multicolor staining [16] and multiwash technique. However these techniques all require special experimental facilities and equipment.

II. IMAGE REGISTRATION WORKFLOW

Image registration has been extensively studied in many applications such as medical imaging, geological survey, and computer vision. It can be formulated as an optimization problem by finding the transformation \mathcal{T} between two images I_1 and I_2 to maximize their similarity, i.e.,

$$\mathcal{T} = \arg \max Similarity(\mathcal{T}(I_1), I_2). \quad (1)$$

The cost function is determined by the similarity measure and transformation space. Commonly used similarity measures include mutual information [11], normalized cross correlation, and summed square difference [7], [8]. Transformation spaces include rigid which deals with only rotation and translation and nonrigid transformation which compensates for deformations such as bending, stretching, shearing and warping [3], [14], [5]. Like any optimization process initialization is critical so in many cases rigid registration result serves as initialization for non-rigid registration [4]. For large images with conspicuous deformations, hierarchical multi-resolution registration methods have also been applied in medical imaging applications [1], [10].

¹This is a tissue-specific knockout animal model.

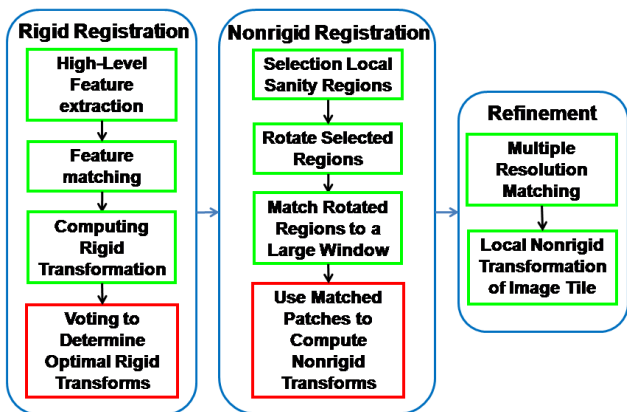


Fig. 1. Image registration workflow. The algorithm consists of three stages: rigid registration, nonrigid registration, and refinement. The green blocks are independent local operations that can be straightforwardly carried out in parallel.

In light microscopy the sectioning process introduces misalignment and relative deformations between adjacent slides and their scans. In addition, adjacent sections can have apparent morphological variations (e.g., the branching of blood vessels). To register images for adjacent sections we use a two stage process that first computes rough alignment and then corrects for deformations and morphological changes using nonrigid transformation as shown in Figure 1. The first stage comes from our previous work on fast rigid registration using high-level features [9] where image regions corresponding to conspicuous anatomical structures such as blood vessels or ducts are matched between images based on properties such as size and shape. These pairs are further filtered based on inter image distances. This process generates large numbers of possible matching features and inevitably includes many mismatches although a significant portion of the corresponding transformations concentrate around the desired rotation and translation parameters in the transformation space. To establish these parameters we adopted a *voting* process that uses the constraints of rigid transformation to robustly discard mismatches. This algorithm is fast and scalable and provides accurate initialization for the nonrigid registration stage.

The task for the nonrigid stage is to establish a set of precisely matched control points that are used to compute a nonrigid transformation which compensates for deformations and morphological changes between the two sections. Matched control points are established by comparing local image intensities at selected conspicuous locations throughout the image. Usually these locations are identified by selecting square patches of pixels with large variance in pixel intensities. These regions are used

as templates and matched with a larger window of pixels in the second image. For each template region in the first image, the location of the matching window in the second image is determined by the rigid transformation. In the large matching window, the patch of pixels with the largest similarity measure to the template region is chosen as its match. Since these matched regions are determined locally instead of globally, incorrect matches can significantly disrupt the overall global matching result and the mechanism to detect incorrect matches is very costly as a global operation on the large images. Thus the classification of correct matches at this stage is critical and it motivates our formulation of a new matching criterion presented in the next section.

Finally, the tissue heterogeneity of the biological samples requires an additional refinement stage for transforming certain regions of interest. For instance, in mouse mammary gland, the adipose tissue and the extracellular matrix around mammary gland ducts have drastically different mechanical properties in terms of elasticity and rigidity. The difference in mechanical properties between these tissues leads to variations in the extent of local deformations in the histological sections. Thus a global nonrigid transformation such as a polynomial transformation is not sufficient to accurately compensate for local deformations and morphological changes. Other methods such as thin-plate spline and local weighted radial functions require a large number of matched control points in this scenario, which is not computationally feasible. Therefore, we identify special regions of interest and conduct a more precise matching in these regions with a multiple resolution fashion to refine the matching accuracy.

III. SHARPNESS OF NORMALIZED CROSS CORRELATION FUNCTION AS A SIMILARITY MEASURE

As discussed in the previous section, establishing control points for nonrigid registration is achieved by matching small patches between images. In many approaches good matches are selected by thresholding the similarity measure such as mutual information (MI) or normalized cross correlation (NCC). MI is often used in cases for comparing images with different modalities or staining, however the computation of MI requires calculation of a 2-D histogram which is very time-consuming. In contrast NCC can be computed very quickly using fast Fourier transform. In this paper we first tested the effectiveness of both measures. In the testing a pair of serial sections were selected, one stained with H+E to

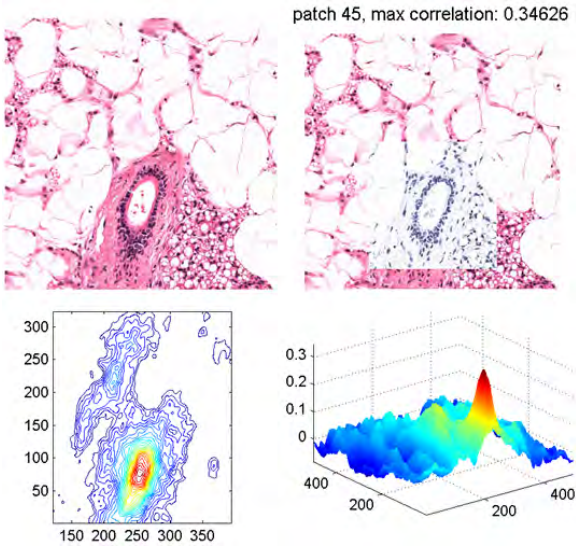


Fig. 2. Example of correct match. Top Left: H+E duct region. Top Right: *PTEN* overlay on H+E corresponding to correlation peak. Bottom Left: Isocontour of the normalized cross-correlation (NCC) function for the duct region between two images with respect to x - and y - translations. Bottom Right: 3-D surface view of the NCC function shows a peak in NCC value.

expose cell nuclei and cytoplasm and the other with immunohistochemical staining for *PTEN*. 320 template regions of 500×500 pixels each were manually selected from ductal areas distributed throughout the H+E image. Their matching regions were also manually identified in the *PTEN* immunohistochemical staining image and a search window of 1000×1000 pixels was designated for each template region. We tested both MI and NCC and visually determined if the maximal similarity measure renders an visually correct match. Figure 2 shows an example of the NCC from one of the pairs used for testing. *Interestingly, in most cases (291 out of 320), the peak location of NCC corresponds to the correct match. This important observation motivated us to investigate further on how to use NCC for matching regions in the case of multiple types of staining due to its low computational cost.*

Next we studied the distribution of maximal NCC values for these region pairs to determine if thresholding could be used to distinguish correct matching results from incorrect ones. As shown in Figure 3, the ranges of NCC values for correct (green points) and incorrect (red points) matches overlaps significantly, indicating that maximal NCC value is not a good candidate for match classification. This is also demonstrated with the pair of regions shown in Figure 4. Although the two pairs have similar peak NCC values, one of the match results is incorrect.

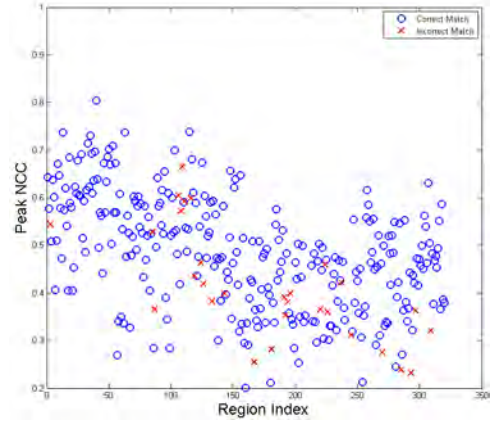


Fig. 3. Peak NCC values for the 320 regions tested.

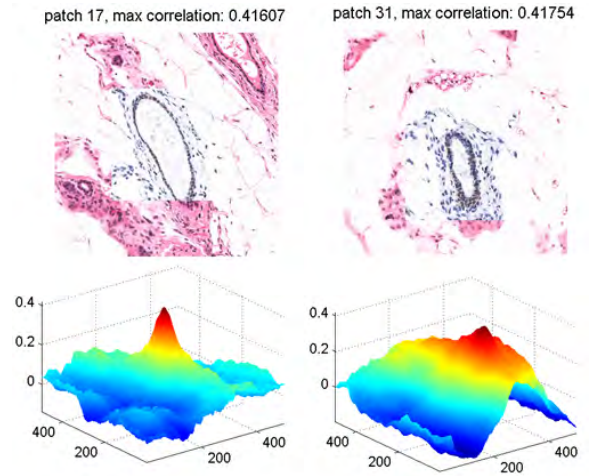


Fig. 4. Examples of correct and incorrect matches. Left: An example of correct match. Right: An example of incorrect match.

Sharpness of the NCC function peak as a similarity measure: We observed in correlations between *PTEN* and H+E staining that although maximal values are not reliable for classifying incorrect matches, a distinguishably sharp peak is observed in most cases where the matching is correct. For this reason we define a sharpness measure based on the cross sectional area of the peak S at different depths h (Figure 5). Specifically our measure is defined as

$$R = h/\sqrt{S}. \quad (2)$$

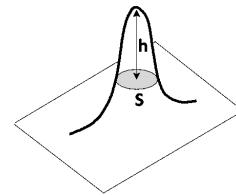


Fig. 5. Illustration of a peak in which h defines the height of the levelset and S defines the area of cross-section at height h .

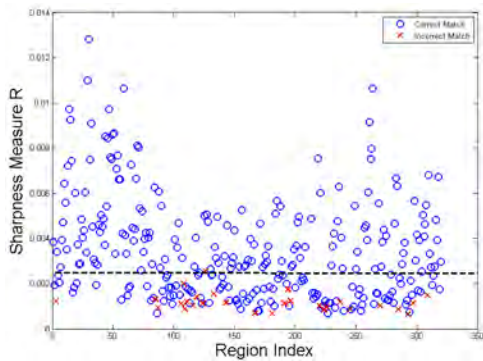


Fig. 6. The distribution of R for 320 regions. Green points represent correctly matched pairs, red points are for falsely matched ones. The dashed line indicates that 0.0025 is a reasonable threshold for discarding most incorrect matches while preserving the majority correct matches.

For fixed depth h , the smaller the cross-section area S , the larger the sharpness measure R is. As shown in Figure 6, thresholding R at 0.0025 can discard most incorrect matches with the cost of discarding some correct matches as well.

IV. MULTIPLE RESOLUTION MATCHING

After the matching, the center points for the template regions and their matches are used as control points to generate global nonrigid transformation such as polynomial or piecewise affine transformation.² However, for the regions of interest such as mammary gland ducts and breast tumor stroma we need to refine the nonrigid transformation to achieve better matching precision. For these selected regions we divided the 500×500 -pixel template patch into four 250×250 -pixel patches and use them for further matching in a smaller searching window. Then piecewise affine transformation is computed and applied to these regions.

V. VALIDATION AND RESULTS

A pair of images as described in Section I was used to test our algorithm. Since no ground truth is available the results were visually inspected and assessed.

The power of using the sharpness measure R as a similarity measure: We computed the ROC curves for thresholding on R and the peak NCC value respectively. As shown in Figure 7, the choice of threshold on R has a fairly large range without incur any false positive

²We did not use other nonlinear transformation such as thin-plate spline or local weighted radial basis function due to the fact that these methods require a larger amount of matching points and the high computational cost to transform the large image.

(between 0.0026 to 0.0039 with at least 100 true positive but no false positive). In practice this is desired since the incorrect matches can disrupt the overall matching.

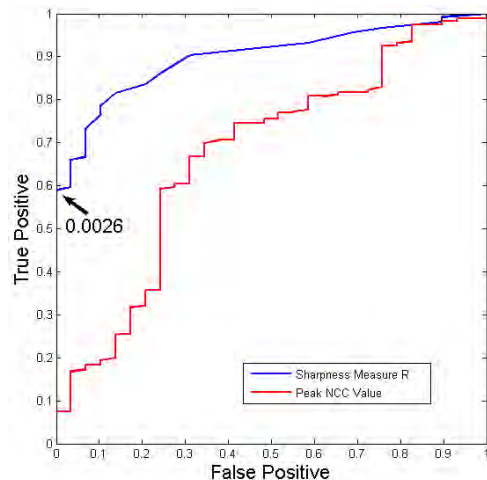


Fig. 7. Comparison of ROC curves for thresholding on the sharpness measure R and on the peak NCC value.

Multiple resolution matching: The goal of the multiple resolution matching is to improve the matching accuracy in key areas of interest. These areas can be either manually selected or automatically chosen based on biological criteria such as cell density or the existence of certain structures. For validation we manually selected 80 regions for testing. Seventy-nine (98.75%) regions show improvement in matching accuracy in terms of continuity and smoothness of the structures. In order to visualize the staining overlay produced by registration we convert the images to gray scale and use the H+E image as the red color channel and the *PTEN* image as the green channel. Overlapping regions of significant intensity appear as yellow. Two examples are shown in Figure 8 and Figure 9. Not only are large structures such as mammary gland ducts overlaid well, microstructures such as cell nuclei and cell membrane are also closely aligned.

Matching of mammary gland ducts: Mammary gland ducts are lined by a layer of epithelial cells which are thought to be the primary sites for breast epithelial tumor initiation. It is critical to have accurate matching for these cells. In most cases the overall mammary gland duct linings are accurate with the layer of epithelial cells tightly overlapped. The individual cell nuclei are not always matched, partially due to the fact that the gap between the two slides is $5\mu\text{m}$ and the nuclei in one section may not appear in the other section. But in general the mapping is accurate within two cells for the inspected regions. The results show that the epithelial

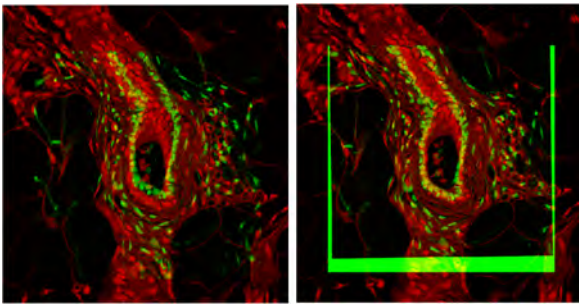


Fig. 8. Visualization of overlay of matched image patches. In order to better visualize the overlapping between two images, we convert both of them into gray scale and put one image in red color channel and another in green color channel. The image intensity values are inverted in order to highlight the stained regions. Left: Overlays of the two images before multiple resolution matching. Right: Overlay of the two images after multiple resolution matching.

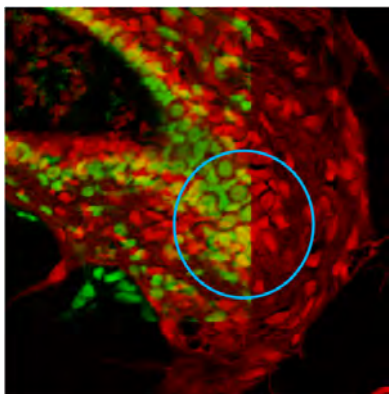


Fig. 9. A zoom in on the overlaid images. The matching of cell nuclei can be seen in the blue circle. However, in most cases we cannot get observe this precise overlapping due to the morphological difference between the two images.

cells have normal *PTEN* expression while the fibroblasts that produce extracellular matrix in the periphery of the ducts are *PTEN* deprived.

As shown in Figure 10, there are usually red regions around the ducts. These regions are mainly composed of fibroblasts and the extracellular matrix (with collagen produced by fibroblasts). These regions are only stained in the H+E image but not the *PTEN* image since *PTEN* gene is inactivated in fibroblasts. However, the epithelial cells which form the lining of the ducts are stained in both sections as shown by the yellow color in the overlaid images, which implies that normal *PTEN* expression in the epithelial cells.

VI. CONCLUSION AND DISCUSSION

In this paper, we propose a new image registration framework for overlaying microscopic images with different types of staining. In order to accurately register

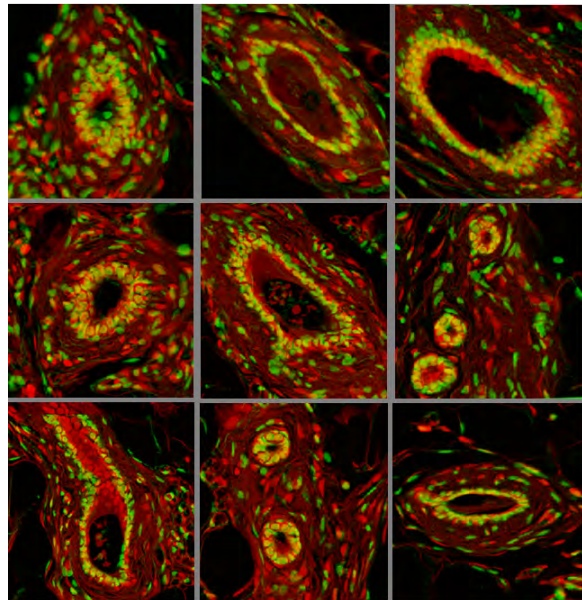


Fig. 10. Examples of matched mammary gland duct areas.

microscopic images, we first established that the sharpness of the normalized cross-correlation function can be used as a similarity measure for matching corresponding points between two images. This helps us to avoid the high computational cost in computing mutual information, which is critical for processing images this large. In order to improve the matching accuracy, we adopt a multiple resolution approach for key regions of interests. The algorithm has been tested using real histological images of mouse mammary gland sample in a breast tumor microenvironment study. The results show that our algorithm is highly accurate. This work lays the foundation for our large scale gene expression mapping of mouse breast tumor microenvironment in which we plan to map expression levels for 50-100 genes over four stages of tumor progression.

Ongoing work includes integration of this algorithm into our parallel MPI framework for NCC matching. This will provide the throughput needed for large scale studies and mapping of other molecules in the tumor microenvironment using the transgenic mouse model.

REFERENCES

- [1] R. Bajcsy and S. Kovacic, "Multiresolution elastic matching," *Computer Vision, Graphics, and Image Processing*, vol. 46, pp. 1–21, 1989.
- [2] G. Bearman and R. Levenson, *Biological Imaging Spectroscopy*. CRC Press, 2003.
- [3] F. Bookstein, "Principal warps: Thin-plate splines and the decomposition of deformations," *IEEE Transactions on Pattern Analysis and Machine Intelligence*, vol. 11, no. 6, pp. 567–585, 1989.

- [4] U. Braumann, J. Kuska, J. Eienkel, L. Horn, M. Luffler, and M. Huckel, "Three-dimensional reconstruction and quantification of cervical carcinoma invasion fronts from histological serial sections," *IEEE Transactions on Medical Imaging*, vol. 24, no. 10, pp. 1286–1307, 2005.
- [5] W. Crum, T. Hartkens, and D. Hill, "Non-rigid image registration: Theory and practice," *The British Journal of Radiology*, vol. 77, pp. S140–S153, 2004.
- [6] C. Eng, "Pten: one gene, many syndromes," *Human Mutation*, vol. 22, no. 3, pp. 183–198, 2003.
- [7] A. Goshtasby, *2-D and 3-D Image Registration: For Medical, Remote Sensing, and Industrial Applications*. Wiley-Interscience, 2005.
- [8] J. Hajnal, H. Derek, and D. Hawkes, *Medical Image Registration*. CRC, 2001.
- [9] K. Huang, L. Cooper, A. Sharma, and T. Pan, "Fast automatic registration algorithm for large microscopy images," in *Proceedings of the IEEE/NLM Life Science Systems & Applications Workshop*, 2006, pp. 1–2.
- [10] M. Lefebvre and L. Cohen, "A multiresolution algorithm for signal and image registration," in *Proceedings of IEEE International Conference on Image Processing*, 1997, pp. III: 252–255.
- [11] F. Maes, A. Collignon, D. Vandermeulen, G. Marchal, and P. Suetens, "Multimodality image registration by maximization of mutual information," *IEEE Transactions on Medical Imaging*, vol. 16, no. 2, pp. 187–198, 1997.
- [12] R. Marc and B. Jones, "Molecular phenotyping of retinal ganglion cells," *Journal of Neuroscience*, vol. 22, no. 2, pp. 413–427, 2002.
- [13] M. Ohara, H. Yeo, F. Savino, G. Iyengar, L. Gong, H. Inoue, H. Komatsu, V. Sheinin, S. Daijavad, and B. Erickson, "Real time mutual information-based linear registration on the cell broadband engine processor," in *Proceedings of the IEEE International Symposium on Medical Imaging (ISBI)*, 2007, pp. 33–36.
- [14] K. Rohr, *Landmark-Based Image Analysis: Using Geometric and Intensity Models*. Springer, 2007.
- [15] H. Sugimoto, T. Mundel, M. Kieran, and R. Kalluri, "Identification of fibroblast heterogeneity in the tumor microenvironment," *Cancer Biology & Therapy*, vol. 5, no. 12, pp. 1640–1646, 2006.
- [16] R. van Vlierberghe, M. Sandel, F. Prins, L. van Iersel, C. van de Velde, R. Tollenaar, and P. Kuppen, "Four-color staining combining fluorescence and brightfield microscopy for simultaneous immune cell phenotyping and localization in tumor tissue sections," *Microscopy Research and Technique*, vol. 67, no. 1, pp. 15–21, 2005.